Narrow sidebranch arrays for low frequency duct noise control

S. K. Tang[a)]
Department of Building Services Engineering, The Hong Kong Polytechnic University, Hong Kong

(Received 12 January 2012; revised 11 September 2012; accepted 14 September 2012)

The present study investigates the sound transmission loss across a section of an infinitely long duct where one or more narrow sidebranch tubes are installed flushed with the duct wall. The finite-element method is used to compute the wave propagation characteristics, and a simplified theoretical analysis is carried out at the same time to explain the wave mechanism at frequencies of high sound reduction. Results show that the high sound transmission loss at a particular frequency is due to the concerted actions of three consecutive sidebranch tubes with the most upstream one in the resonant state. The expansion chamber effect of the setup also plays a role in enhancing sound attenuation at non-resonance frequencies. Broadband performance of the device can be greatly enhanced by appropriate arrangements of tube lengths and/or by coupling arrays on the two sides of the duct.
 [http://dx.doi.org/10.1121/1.4756951]

PACS number(s): 43.50.Gf, 43.20.Mv [DKW] Pages: 3086–3097

I. INTRODUCTION

Ventilation and air conditioning systems are an important mechanical component of modern buildings. These systems consist mainly of air handling units, fans, and extensive ductwork. Used air is extracted from the occupied spaces, treated, and conveyed back to the occupants to maintain good air quality and thermal comfort. However, the noise from the system propagates into the occupied zones through the ductwork, affecting the acoustical environment indoor.[1] There have been efforts attempting to restrict/control the noise exposure of the building occupants (for instance, Beranek[2] and Blazier[3]).

The traditional method for air conditioning noise control is the use of dissipative silencers in which the sound absorption materials in the silencers dissipate the sound energy into heat.[4] However, these silencers are not effective at lower frequencies because of the acoustical properties and the damping mechanism of the sound absorption materials. They also result in a significant static pressure drop in the ductwork that must be overcome by extra fan power before the designed air flow rate can be delivered. This extra fan power requirement leads to the installation of more powerful (and noisy) fans, which in turn increase the burden of the silencing devices. In addition, the porous sound absorption materials cannot be used in areas under stringent hygiene control, such as hospitals, or when the air is dirty and/or greasy. There are efforts in the study of active noise control.[5] Although the concept has been successfully implemented in practice, the reliability of the sensors in the relatively hostile environment inside the air conditioning ductwork remains an important engineering challenge. The use of acoustic-membrane interaction has also been introduced recently by Huang and Choy,[6] but keeping the membrane in the right tension practically is not a simple task.

Passive reactive silencing devices that contain no flexible structures are often used in practical noise control because of more stable performance. The Helmholtz resonators[7] and the plenum chambers[8] are typical examples. There are many derivatives proposed as well. Examples include the resonators with extended necks,[9] coupled resonators,[10–12] the conical tube resonator,[13] and the Herschel–Quincke tubes,[14] and this list is far from exhaustive. However, these devices can give very good sound reduction performance only at the resonance frequencies or within a relatively narrow frequency range around those frequencies. Coupling up resonators can improve the bandwidth of the sound attenuation as shown in Seo and Kim[10] and Howard *et al.*[15] However, the distribution of the resonance frequencies of the resonators must be carefully selected. A more systematic method for estimating the required resonance frequencies of the individual resonators is needed.

Sidebranches with lengths comparable to the width of the main duct perform somewhat like an expansion chamber.[16] However, a narrow sidebranch tube with its mouth flushed with the duct wall will give a performance somewhat similar to that of a Helmholtz resonator when it resonates. The narrow width of the sidebranch tube ensures longitudinal wave motions along its length, and its resonance frequencies can readily be approximated using the branch length. Coupling up narrow sidebranches is expected to be at least more space-effective than coupling up Helmholtz resonators for the same noise reduction bandwidth. The major aim of the present study is to examine the sound transmission loss across narrow sidebranch tube arrays and the arrangement of the sidebranch lengths for broadband noise reduction performance. The finite-element method will be adopted as in the previous studies of the author (for instance, Tang[16] and Lau and Tang[17]). As the low frequency issue is more important in building noise control, this study is focused at frequencies below the first higher mode cut-off frequency of the main duct.

II. THEORETICAL CONSIDERATIONS

This section summarizes a simplified theoretical model for investigating the potential sound transmission loss of a

[a)]Author to whom correspondence should be addressed. Electronic mail: shiu-keung.tang@polyu.edu.hk

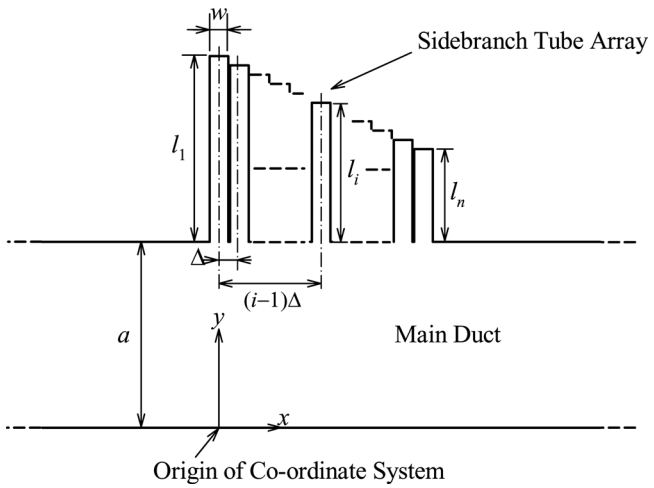

FIG. 1. Schematics and nomenclature adopted in the present study.

narrow sidebranch array and the underlying physical wave interactions leading to the transmission loss. Figure 1 illustrates an array that consists of n number of narrow sidebranch tubes (length l_i, $i=1, 2,\ldots, n$) installed flush with the upper wall of an infinitely long duct of width a. The sidebranch tube width in the spanwise direction is the same as that of the duct, so that the present problem is two dimensional as there is no excitation in the spanwise direction.[17,18] The present study is focused at frequencies below the first higher mode cut-off frequency of the main duct, such that only plane waves can travel along the sidebranch tubes and along the main duct at locations far away from the sidebranch tube array. However, higher modes in the forms of evanescent waves exist in the proximity of the array. For simplicity, the widths of the sidebranch tubes are set equal to w, and the separation between two adjacent sidebranch tube center line Δ.

Without loss of generality, one can set the location of the first sidebranch center line L_1 at $x/a=0$, that is $L_1/a=0$, such that $L_i=(i\text{-}1)\Delta$. As the sidebranch tubes are narrow, the higher mode contribution along the tubes should be negligibly weak within the frequency range of the present study. The air movement at the mouth of each sidebranch tube is assumed uniform and planar with a sinusoidal velocity $V_i e^{j\omega t}$ similar to a vibrating air piston (ω the angular frequency). The sound pressure at any point (x,y) along the infinitely long two-dimensional duct, $p(x,y)$, created by this single air piston vibration at the mouth of the ith sidebranch tube is, ignoring the viscous damping action:[19,20]

$$p(x,y)=\frac{\rho c_0}{2a}\sum_{m=0}^{\infty}(2-\delta_{0m})(-1)^m c_m V_i \times\cos\left(\frac{m\pi y}{a}\right)\int_{L_i-w/2}^{L_i+w/2}[H(x-x')e^{-jk(x-x')/c_m}+H(x'-x)e^{jk(x-x')/c_m}]dx', \tag{1}$$

where ρ is the ambient air density, δ and H denote the Kronecker delta function and the Heaviside step function, respectively, and k is the wavenumber and $k=\omega/c_0$ with c_0 representing the ambient speed of sound, which equals that of the plane wave propagation. The modal wave speed, after normalization by c_0, is

$$c_m=\frac{k}{\sqrt{k^2-(m\pi/a)^2}}, \tag{2}$$

for $m\geq 1$. At frequency below the first cut-off frequency of the main duct, c_m is complex and equals $j|c_m|$ for $m\geq 1$. After integration, Eq. (1) becomes

$$p(x,y)=\frac{\rho V_i c_0}{ka}\left[\sin\left(\frac{kw}{2}\right)e^{-jk|x-L_i|}-2j\sum_{m=1}^{\infty}(-1)^m|c_m|^2 \times\cos\left(\frac{m\pi y}{a}\right)\sinh\left(\frac{kw}{2|c_m|}\right)e^{-(k/|c_m|)|x-L_i|}\right], \tag{3}$$

and for the sake of easy presentation, we define

$$G(x,y|L_i,a)=\frac{\rho c_0}{ka}\left[\sin\left(\frac{kw}{2}\right)e^{-jk|x-L_i|}-2j\sum_{m=1}^{\infty}(-1)^m|c_m|^2 \times\cos\left(\frac{m\pi y}{a}\right)\sinh\left(\frac{kw}{2|c_m|}\right)e^{-(k/|c_m|)|x-L_i|}\right] \tag{4}$$

and thus $p(x,y)=V_i G(x,y|L_i, a)$. The fluid loading in term of average pressure acting on a single air piston at the mouth of a sidebranch tube can be determined theoretically as in Huang:[20]

$$\bar{p}=\frac{\rho c_0 V_i}{jka}\left[1-e^{-jkw/2}\frac{\sin\left(\frac{kw}{2}\right)}{\frac{kw}{2}}\right]+2j\,\frac{\rho c_0 V_i}{ka}\sum_{m=1}^{\infty}|c_m|^2 \times\left[1-e^{-kw/2|c_m|}\frac{\sinh\left(\frac{kw}{2|c_m|}\right)}{\frac{kw}{2|c_m|}}\right]=V_i F, \tag{5}$$

and F is the same for all sidebranch tubes and its magnitude is small if w/a is small. The average air pressure at the mouth of the ith sidebranch tube is

$$\frac{1}{w}\int_{L_i-w/2}^{L_i+w/2}\left[Ie^{-jkx}+\sum_{\substack{j=1\\ j\neq i}}^{n}V_j G(x,a|L_j,a)\right]dx+V_i F=Z_i V_i, \tag{6}$$

where Z_i is the acoustic impedance at the mouth of the ith sidebranch tube and I the amplitude of the incident plane wave in the main duct. The terms in the summation on the left-hand side of Eq. (6) represent the contributions from the other sidebranches. As planar air movements at the mouths of the sidebranch tubes are assumed, it is known, for pure plane wave propagation inside the sidebranch tube, that $Z_i=-j\rho c_o\cot(kl_i)$.[21] Also,

$$\int_{L_j-w/2}^{L_j+w/2} G(x,a|L_i,\,a)dx = \int_{L_i-w/2}^{L_i+w/2} G(x,\,a|L_j,\,a)dx$$
$$= \frac{\rho c_0}{ka}\left(\frac{\sin^2\left(\frac{kw}{2}\right)}{k/2}e^{-jk|L_j-L_i|} - 2j\sum_{m=1}^{\infty}|c_m|^2\frac{\sinh^2\left(\frac{kw}{2|c_m|}\right)}{k/(2|c_m|)}e^{-(k/|c_m|)|L_j-L_i|}\right), \tag{7}$$

and V_i can be obtained by solving the n simultaneous equations:

$$\begin{pmatrix} \alpha_{11} & \cdots & \alpha_{1n} \\ \vdots & \ddots & \vdots \\ \alpha_{1n} & \cdots & \alpha_{nn} \end{pmatrix}\begin{pmatrix} V_1 \\ \vdots \\ V_n \end{pmatrix} = \begin{pmatrix} J_1 \\ \vdots \\ J_n \end{pmatrix}, \tag{8}$$

where

$$J_i = \frac{1}{w}\int_{L_i-w/2}^{L_i+w/2} Ie^{-jkx}dx = I\frac{\sin\left(\frac{kw}{2}\right)}{kw/2}e^{-jkL_i} \tag{9}$$

and

$$\alpha_{ij} = \begin{cases} -\frac{1}{w}\int_{L_j-w/2}^{L_j+w/2} G(x,a|L_i,a)dx & \text{for } i \neq j \\ Z_i - F & \text{for } i = j. \end{cases} \tag{10}$$

The corresponding analytical forms of V_is are very tedious[22] and in principle not essential for the following discussions. The overall sound field far downstream of the sidebranch array is, as far as $ka < \pi$,

$$p_{x\to\infty} = \left(I + \frac{\rho c_0}{ka}\sin\left(\frac{kw}{2}\right)\sum_{i=1}^{n} V_i e^{jkL_i}\right)e^{-jkx}. \tag{11}$$

The case for $n=3$ is examined in detail in the following analysis in this section for an understanding of the wave behaviors at two important and critical situations. These pieces of information will be further discussed in Sec. IV and will assist the interpretation of the finite-element calculation results. For $n=3$, there are two cases of $p_1 \approx 0$ worth attention. The first one is the case where $V_1 \approx 0$ and thus $\partial p/\partial y$ at the mouth of the first sidebranch is very small. The first sidebranch behaves like a hard wall. With $V_1 \to 0$, $\alpha_{12}V_2 + \alpha_{13}V_3 = I$ and for narrow sidebranch tubes ($kw \to 0$ and $w/a \to 0$) which are closely packed together ($k\Delta \to 0$),

$$I + \frac{\rho c_0 w}{2a}(1-jk\Delta)V_2 - \rho w j V_2 c_0 \sum_{m=1}^{\infty}\frac{|c_m|}{a}\left(1 - j\frac{k\Delta}{|c_m|}\right)$$
$$+ \frac{\rho c_0 w}{2a}(1-2jk\Delta)V_3 - \rho w j V_3 c_0 \sum_{m=1}^{\infty}\frac{|c_m|}{a}\left(1 - 2j\frac{k\Delta}{|c_m|}\right) \approx 0, \tag{12}$$

and thus V_2 and V_3 are in anti-phase relationship with the former having a higher magnitude. By considering the leading order term, one obtains

$$I + \frac{\rho c_0 w}{2a}(V_2+V_3) \approx \rho w j (V_2+V_3) c_0 \sum_{m=1}^{\infty}\frac{|c_m|}{a}. \tag{13}$$

One can then conclude using Eq. (11) that the far field pressure $p_{x\to\infty}$ will not vanish and a high sound transmission loss is not likely in this case. It will be discussed further in Sec. IV.

The second case of interest is the one where very high sound transmission loss is achieved (that is, $p_{x\to\infty} \to 0$). One can notice from Eqs. (6), (8), and (11) that again for the case of $kw \to 0$, $w/a \to 0$, and $k\Delta \to 0$,

$$Z_1 \approx j\rho c_0 \sum_{m=1}^{\infty}\frac{W|c_m|}{a}\left(1 - \frac{V_2}{V_1}e^{-k\Delta/|c_m|} - \frac{V_3}{V_1}e^{-2k\Delta/|c_m|}\right)$$
$$\Rightarrow |Z_1| \to 0, \tag{14}$$

then

$$I + \frac{\rho c_0 w}{2a}[V_1 + V_2(1-jk\Delta)$$
$$+ V_3(1-2jk\Delta) + O((k\Delta)^2)] \approx 0. \tag{15}$$

The condition shown in Eq. (14) implies that the acoustic pressure at the mouth of the first sidebranch tube is very weak. However, the corresponding acoustic velocity is finite and can be strong under resonance. One can deduce by considering the coefficient of the first order $k\Delta$ term in Eq. (15) that V_2 and V_3 should be nearly in anti-phase and $|V_2| > |V_3|$. The corresponding leading order term then tends to suggest that V_1 and V_3 should be roughly in phase as the magnitude of V_1 compared to that of the acoustical particle velocity induced by the incident wave is very large due to resonance. At this condition of vanishing sound power transmission across the array, the first tube is resonating ($|Z_1| \to 0$), while the second and the third tubes are creating a dipole action. A portion of the latter tends to cancel the phase difference effects resulted from the spatial separation between the second and the third sidebranch tubes. One should note that the preceding does not apply to the condition where the resonance occurs along the second sidebranch tube, suggesting that such resonance will not result in strong sound attenuation in general. The preceding conclusion should apply to sidebranch arrays installed symmetrically on the upper and lower duct walls and for $n > 3$. More discussions will be given in Sec. IV.

The viscous damping[23] at the mouths of the sidebranch tubes is ignored in the present study. It is expected that such effect will reduce the sharpness of the resonance and affect the resonance frequencies. However, it is likely that such

effect will improve operating bandwidth while maintaining reasonable noise attenuations of coupled resonating devices,[24] and thus the viscous effect may be beneficial to the sidebranch array provided that the widths of the sidebranch tubes are not very narrow, although the sound transmission loss will be lowered. The viscous damping could also weaken the non-planar components of the air motion at the mouth of each sidebranch tube. These are left to further investigation.

It is observed that the sidebranch tube array can provide a very broadband sound transmission loss (*TL*) if the array consists of many narrow sidebranch tubes of very small length variation. However, this will result in an unnecessarily long device that is not going to be practical. The coupled resonators of Howard *et al.*[15] are very long. In the present study, the length of the sidebranch tube array is restricted to within approximately 1-3 duct widths for practical purpose.

III. THE COMPUTATIONAL MODEL

The analysis commences with a rigid walled sidebranch tube array mounted on one side of the duct as shown in Fig. 1. The width of the sidebranch tubes in the present study varies between $0.05a$ and $0.2a$. The length of the longest (the first also) sidebranch tube is set at a and that of the shortest one (the last tube) at $a/2$, giving a working frequency range roughly between $0.5f_c$ to f_c, where f_c is the first higher mode cut-off frequency of the main duct. The gap between adjacent sidebranch tubes is fixed at $0.01a$. The upstream end of the computation domain is set at $x/a=-5$, while the downstream end of the domain is at $x/a=6$, which is at least $3a$ downstream of the last sidebranch tube such that all evanescent waves should have significantly decayed even they are generated by the sidebranch array. The sound transmission loss across the sidebranch array can be estimated by solving the standard wave equation

$$\nabla^2 p + k^2 p = 0 \tag{16}$$

by the finite-element method implemented using the software MATLAB as in Tang.[17] The finite-element method can cater for any non-planar air motions at the mouths of the sidebranch tubes and thus should be more accurate than the simplified theory in Sec. II. Below f_c, the waves sufficiently far away from the array are essentially planar. For a unit strength plane excitation at $x/a=-5$, the boundary conditions at the two ends of the computation domain are[16,17]

$$\frac{dp}{d\hat{n}} + jkp = \begin{cases} 2jk & at \quad x/a = -5 \\ 0 & at \quad x/a = 6\,, \end{cases} \tag{17}$$

where $\hat{n}$ denotes the unit outward normal of the computational domain boundary. The condition at $x/a=-5$ denotes the presence of a unit strength plane excitation wave at the upstream computational domain boundary, while the one at $x/a=6$ represents an outgoing plane wave condition. The normal acoustic velocities vanish at all other surfaces.

The situation for two sidebranch arrays mounted symmetrically on the upper and lower duct walls is very much similar to those described in the preceding text except that the waves far enough from the arrays will still be planar for $ka<2\pi$ if the two arrays are identical as there will be no odd mode excitation below such wavenumber. The length of the last (also the shortest) sidebranch tube in these cases is $a/4$. It will be shown later that identical arrays are more effective than the asymmetric array setup in term of sound transmission loss.

The finite-element computations in the present study are done using the partial differential equation (PDE) solver and the mesh generation engine of the software MATLAB.[25] The Delaunary triangulation algorithm is used to generate the meshes.[26] The mesh sizes vary with the sidebranch array configurations. The minimum node points per wavelength and the triangle quality are kept above 6 and 20, respectively, throughout the present study as in Tang.[17] It has been confirmed that any further refinement of the meshes will not give noticeable difference in the computed results.

Under the present length restriction, the axial variation of the sidebranch tube lengths will play a very important role in affecting the broadband *TL* characteristics of the array as it controls the axial variation of acoustic impedance across the array. Two length variations are chosen for detailed investigation. The first one is a linear model where the length of the ith sidebranch tube is

$$l_i = l_{max} - (l_{max} - l_{min})\frac{i-1}{n-1}, \tag{18}$$

and the other is so chosen that the undamped fundamental resonance frequency difference between two adjacent sidebranch tubes without fluid loading is a constant such that

$$\frac{1}{l_i} = \frac{1}{l_{max}} + \frac{i-1}{n-1}\left(\frac{1}{l_{min}} - \frac{1}{l_{max}}\right). \tag{19}$$

There are many other possible simple forms for the sidebranch tube length variation. One can think of the exponential, conical, and cubic length variations. It will be shown later that the exponential one gives a performance similar to that of the form described by Eq. (19). The conical and cubic variation forms result in relatively rapid change in the sidebranch tube resonance frequency at some locations along the length of the sidebranch array; this is not favorable for broadband sound attenuation in principle. Thus they are not considered in detail in the present study. The arrays with linear tube length variation [Eq. (18)] and linear frequency variation [Eq. (19)] are denoted hereinafter as the L-type and F-type array, respectively. In the following discussions, $l_{max}=l_1=a$ and l_{min} is the length of the last tube in a sidebranch array.

IV. RESULTS AND DISCUSSIONS

The results presented in this section are mainly from finite-element computations. Before detail discussions, a comparison between the theoretical prediction from the simplified model in Sec. II [obtained by solving Eqs. (6) and (11)] and the finite-element computations for the 11 sidebranch tube L-type array with $w=0.1a$ and $l_{11}=0.5a$ is presented in Fig. 2. One can observe that the simplified theoretical model, although it has not fully taken into account the coupling

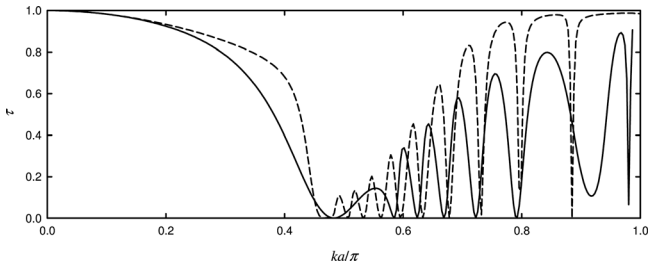

FIG. 2. Comparison between simplified theoretical prediction and finite-element simulation for the array with $w = 0.1a$, $l_{11} = 0.5a$ and 11 sidebranch tubes. —, theoretical prediction; - - -, finite-element simulation.

between sidebranches, gives a prediction that is largely in-line with the finite-element result, confirming the basic performance of the array. The former appears to have overpredicted the transmission loss at higher frequencies, probably due to the presence of non-planar air motions at the mouths of the sidebranch tubes that tend to reduce the radiation efficiency there except at the point of resonance. It should be noted that the simplified theoretical model is not so valid toward the first higher mode cut-off frequency of main duct ($ka \to \pi$). Results of other cases are similar and thus are not presented.

Figure 3(a) illustrates the frequency variations of the sound power transmission coefficients, τ, across the L-type and F-type arrays with $w = 0.1a$, $l_{11} = 0.5a$ (11 sidebranch tubes). The results of the exponential and cubic length variations are also included for comparison. The total longitudinal lengths of the arrays are roughly $1.2a$. The performance of the cubic length variation is the worst probably because of the rapid change in the sidebranch resonance frequencies at middle of the array. One can observe that for all other the length variations, a relatively broadband attenuation of over 10 dB ($\tau < 0.1$) can be achieved at the lower end of the array working bandwidth, while discrete and narrow band sound attenuations are observed on the opposite side of the array bandwidth. The F-type array appears to be slightly better than the L-type array in term of the bandwidth of high sound attenuation. Because the exponential length variation setup gives a performance very similar to that of the F-type array, the following discussions will be focused on the linear length variation and liner resonance frequency variation models.

Figure 3(b) shows the frequency variation of *TL* of the arrays considered in Fig. 3(a). One can notice that the L-type array performs better than the F-type array within roughly the first half of the array working bandwidth, and the opposite occurs within the other half of the array working bandwidth. Therefore there is a possibility of combining these two array types for enhanced broadband sound attenuation performance. This will be discussed later.

Figures 4(a)–4(c) illustrate, respectively, the distributions of acoustic pressure magnitudes, sound pressure, and the transverse acoustic particle velocity at $ka = 2.13$ for the L-type array considered in Fig. 3. This is the frequency at which $\tau \approx 0$ [Fig. 3(a)]. The acoustic pressure magnitude at the mouth of the sixth sidebranch tube is very weak, but the acoustic particle velocity there is finite. The length of this sidebranch tube l_6 is $0.75a$ and thus $kl_6 = 1.598 \approx \pi/2$, indicating that a "one-end-opened-one-end-closed" type tube resonance occurs along this sidebranch tube. Figures 4(b) and 4(c) show, respectively, the relationships between the acoustic pressures and the real parts of the transverse acoustic particle velocities of the sixth, seventh, and eighth sidebranch tubes. The imaginary parts of the transverse acoustic particle velocities show very similar characteristics as their real parts and thus are not presented. These observations are in line with those predicted in Sec. II. The air vibrations inside the seventh and eighth sidebranch tubes interfere destructively with each other at locations close to the region between the mouths of

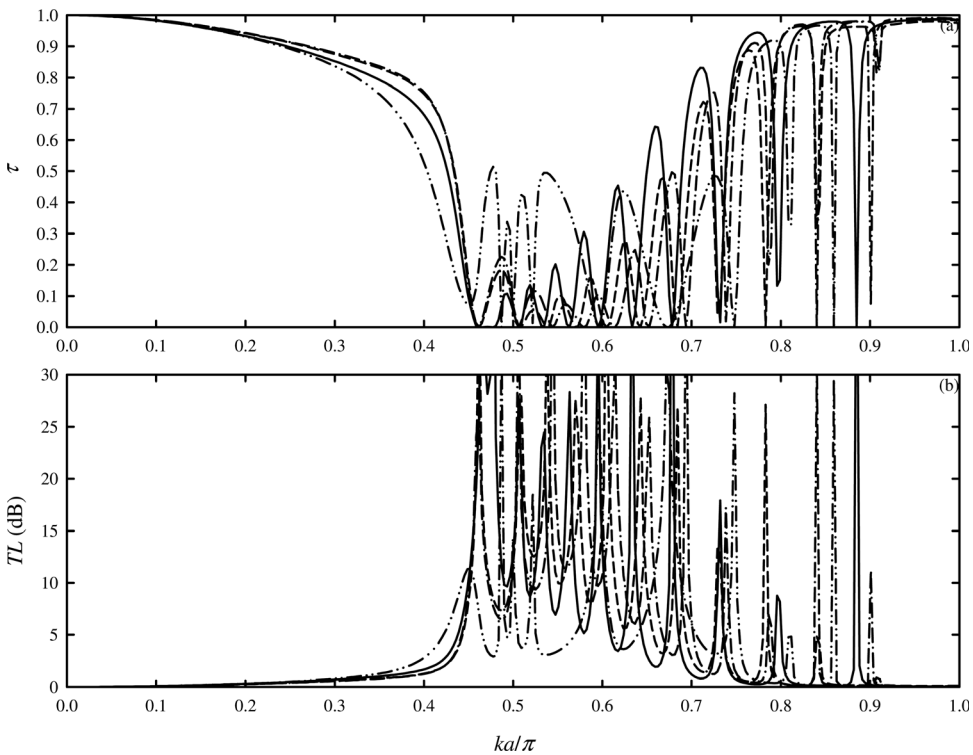

FIG. 3. Sound transmissions across arrays of various tube length arrangements. (a) Sound power transmission coefficients of arrays; (b) sound transmission losses across arrays. $w = 0.1a$, $l_{11} = 0.5a$ with 11 sidebranch tubes. —, L-type; - - -, F-type; - · -, exponential length variation; - · · -, cubic length variation.

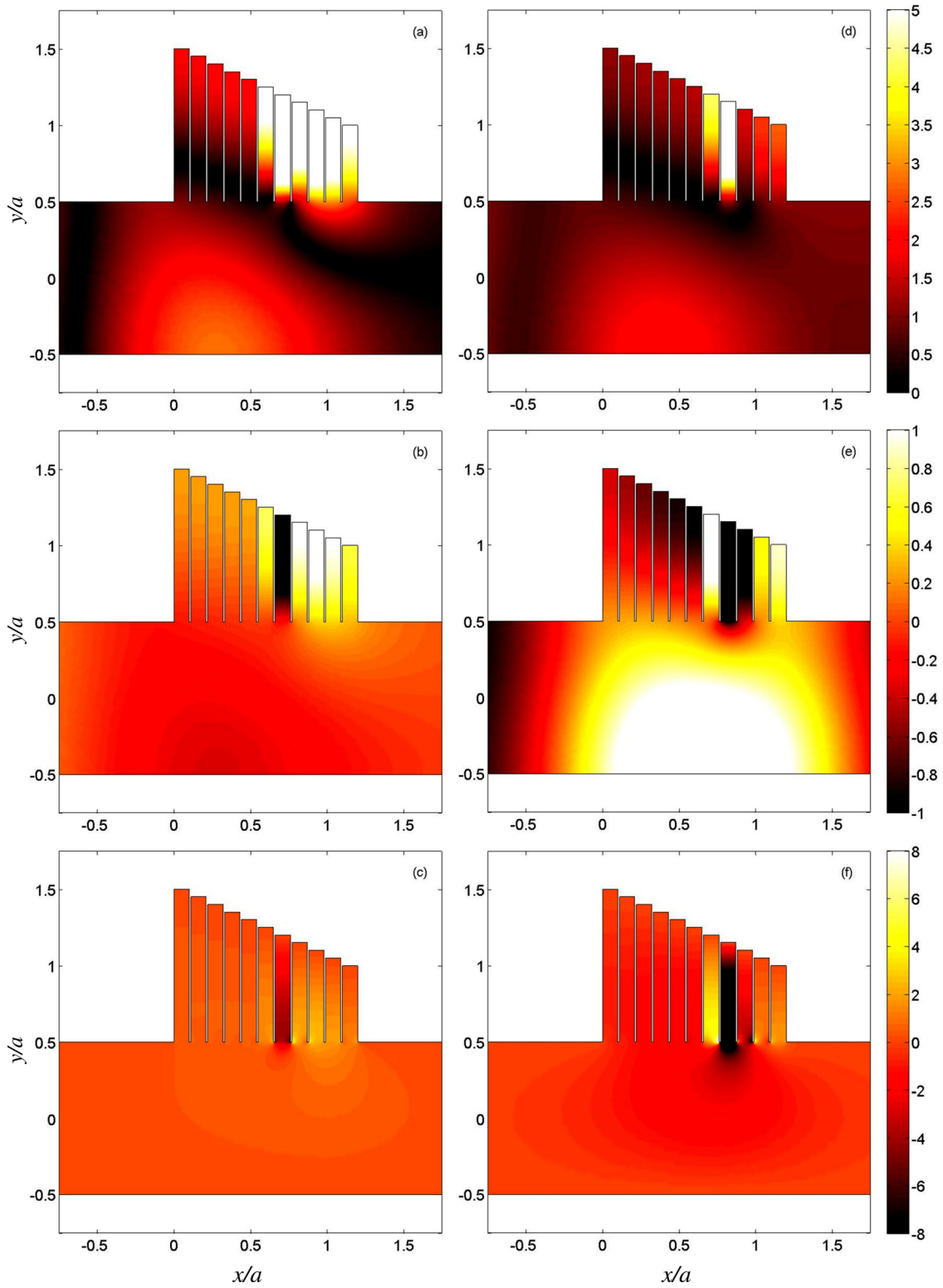

FIG. 4. (Color online) Wave patterns within L-type array with 11 tubes, $w = 0.1a$, $l_{11} = 0.5a$. (a) Acoustic pressure magnitude at $ka = 2.13$. (b) Real part of the acoustic pressure at $ka = 2.13$. (c) Real part of the transverse acoustical velocity at $ka = 2.13$. (d) Acoustic pressure magnitude at $ka = 2.24$. (e) Real part of the acoustic pressure at $ka = 2.24$. (f) Real part of the transverse acoustical velocity at $ka = 2.24$.

these sidebranch tubes. This dipole sound interacts with the incident wave and the sound generated by the first sidebranch tube, resulting in very low acoustic pressure downstream of the sidebranch array. It is also observed that the transverse particle velocities inside the sidebranch tubes are basically in phase except for that within the sidebranch tube immediately downstream of the resonating one (seventh sidebranch tube in this case), which is in anti-phase with those inside the other sidebranch tubes. The acoustic pressure magnitudes inside the sidebranch tubes before the resonating sidebranch tube are weak, while those after that tube are strong. The preceding observations apply to other frequencies at which a dip of τ to

nearly 0 is found, except the first one at $ka = 1.50$, which is due mainly to the macroscopic expansion chamber effect (discussed later). It can be concluded that the large sound attenuations of the sidebranch tube array are achieved basically through the actions of three adjacent sidebranch tubes, which is in line with the theoretical deduction made in Sec. II.

In Figs. 4(d)–4(f) are shown, respectively, the distributions of acoustic pressure magnitudes, sound pressure, and real part of the transverse acoustic particle velocity at $ka = 2.24$ for the L-type array considered in Fig. 3. The sound power transmission coefficient at this frequency is relatively high [Fig. 3(a)]. The acoustic pressure magnitude at the mouth of the seventh sidebranch tube in this case is again weak, but unlike the previous case, the acoustic particle velocity there is also weak. The corresponding velocity (both its real and imaginary parts) at the mouth of the eighth sidebranch tube is very strong and is basically out of phase with that at the mouth of the ninth sidebranch tube. This is again in line with the prediction in Sec. II. However, these strong velocities are only restricted within a small region by the strong pressure inside the main duct, and the overall wave activity can only result in limited sound attenuation. It is interesting to note that $kl_7 = 1.568$, which is very close to $\pi/2$, but the conventional tube resonance has not occurred because of the fluid loading effect, which alters the effective length of the sidebranch tube. Same phenomenon takes place at other frequencies at which a local maximum of τ is found.

Figure 5 illustrates the effects of sidebranch tube width w on τ of the L-type arrays, while the external dimensions of these arrays are kept nearly the same. As the working length of the array is fixed, a smaller w results in more sidebranch tubes in the array and thus more discrete sharp drops in τ within the working bandwidth. It is obvious that the array with the smallest w gives the best broadband performance when the viscous effect is ignored. However, one can notice that there exists a common inverted dumbbell shape slow variation of τ for all w studied. These arrays are basically closed end sidebranches,[16] and the slow variation of τ represents roughly the macroscopic property of the basic sidebranch with an inclined close end, which is not much affected by the individual resonances inside the sidebranch tubes.

Figure 6(a) illustrates the sound magnitude of the L-type array with $w = 0.1a$, 11 tubes and $l_{11} = 0.5a$ at $ka = 1.5$ under the abovementioned expansion chamber effect. This is at the frequency where the first τ dip is observed [Fig. 3(a)].

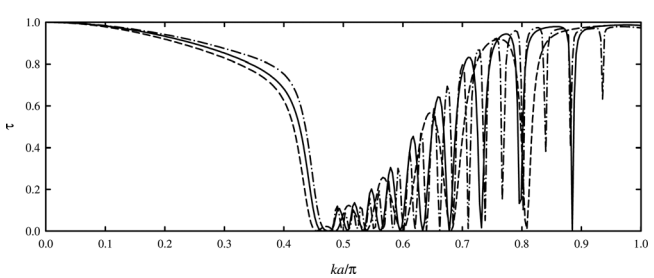

FIG. 5. Effects of sidebranch tube width on sound power transmission coefficients of the L-type arrays with $l_{min} = 0.5a$ and similar total axial lengths. —, $w = 0.1a$, 11 tubes; - - -, $w = 0.2a$, 6 tubes; - · -, $w = 0.05a$, 21 tubes.

One can notice that the sound attenuation is resulted from the combined strong relatively in-phase actions of the first several sidebranch tubes in the array instead of the resonance of an individual sidebranch tube [Fig. 4(a)]. This happens in all the cases studied in this investigation. It is also found that the last τ dip at $ka < \pi$ for each sidebranch array setting included in Figs. 3 and 5 is due to the resonance of the third last sidebranch tube. An example of sound magnitude of the L-type array at $ka = 2.54$ is given in Fig. 6(b) ($w = 0.2a$, 6 tubes and $l_6 = 0.5a$). This is also in line with the theoretical deduction that high sound transmission loss is achieved together with the actions of the two sidebranch tubes immediately downstream of the resonating one. The F-type array exhibits similar characteristics, and thus the corresponding results are not presented.

It has been indicated briefly that the "one-end-opened-one-end-closed" type tube resonance does not take place at $kl_i = \pi$ (Figs. 3 and 5). The end impedance of the sidebranch tube in ducted condition appears to have reduced the

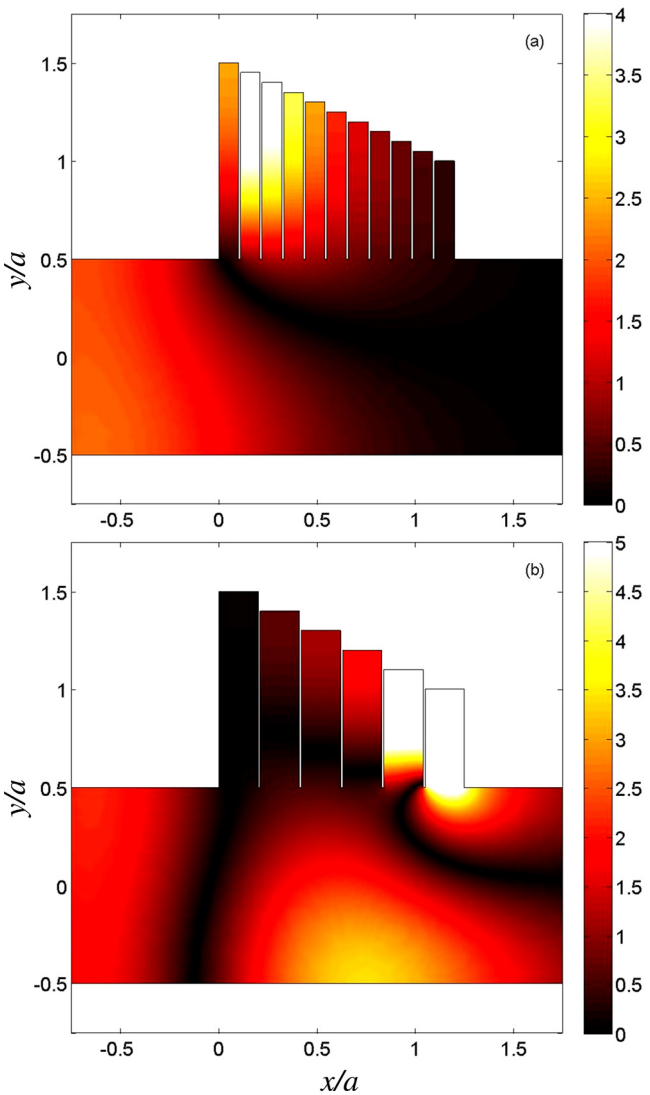

FIG. 6. (Color online) Acoustic pressure magnitudes within the L-type arrays at frequencies of first and last τ dips. (a) $ka = 1.50$, $w = 0.1a$, $l_{11} = 0.5a$, 11 sidebranch tubes. (b) $ka = 2.54$, $w = 0.2a$, $l_6 = 0.5a$, 6 sidebranch tubes.

effective length of the tube at resonance. In Fig. 7 are presented the effective lengths, l_e, of the sidebranch tubes at resonance for the sidebranch arrays with total longitudinal lengths of $\sim 1.2a$. For the L-type array, l_e varies roughly linearly with the tube length, and the smaller the tube width w, the smaller the difference between the two lengths (length difference). For the case of $w = 0.05a$, the length differences are insignificant. One can also notice from Fig. 7 that the length difference is smaller for the case of a shorter physical tube length. The F-type array results clearly in non-linear variation of l_e with the physical tube length. Again the length difference increases with tube width. However, unlike the L-type array, the length difference for the F-type array increases with physical tube length. It should be noted that the variation of physical tube length at the rear region of the F-type array (with shorter sidebranch tubes) is small, while that at the initial region of the array is relatively rapid. Observing that the acoustic impedance of the sidebranch tube is $-j\rho c_o \cot(kl)$, if one ignores the fluid loadings at the tube mouth, it is reasonable to believe that the larger longitudinal impedance variation in the initial region of the array has resulted in stronger reflection of acoustic energy and thus a larger negative length difference/correction. Such phenomenon is much less serious for the L-type array setting. Because the rate of tube length variation at the rear part of the F-type array is lower than that of the L-type array of the same w, the former results in insignificant length differences for $l < 0.75a$ except for $w = 0.2a$. However, the corresponding differences for the $w = 0.2a$ case are still small.

Because only three adjacent sidebranch tubes are mainly responsible for the wave behaviors under resonance, the total length of the sidebranch array does not have significant effect on the length difference as far as the tube width and the longitudinal rate of change of tube length are fixed (not presented here). It should be noted that the presence of air viscosity can result in higher impedances at the mouths of the sidebranch tubes, and it is very likely that very small w is actually undesirable to sound attenuation. This is left to further experimental study.

One can notice from Fig. 5 that the τ dips of the $w = 0.1a$ array ($l_{11} = 0.5a$, 11 tubes) appear basically between two adjacent τ dips of the $w = 0.2a$ array ($l_6 = 0.5a$, 6 tubes). The broadband sound transmission loss is greatly enhanced when these two sidebranch arrays (L-type) can be applied together as illustrated in Fig. 8. The sub-figure in Fig. 8 shows the configuration of the combined array. A broadband attenuation within $0.48 < ka < 1.0$ can be achieved, while those across the range $0.48\pi < ka < 0.77\pi$ are very impressive with τ less than 0.05 even at those frequencies where only limited sound attenuations can be achieved by the individual arrays. Figures 9(a)–9(c) illustrate, respectively, the sound pressure field, the transverse, and the longitudinal acoustic particle velocity distributions within the combined array at $ka = 2.39$. This is the frequency at which the sound power transmission coefficients of individual arrays are greater than 0.9, that is, close to the frequency of $V_2 = 0$ of the three tube array example given in Sec. II. While the pressure fluctuations on the two sides of the main duct are nearly in phase, the particle velocities are of opposite directions but similar strengths. Strong velocities toward the duct axis are observed at the mouths of the sidebranch tubes at $x/a = 1$. They are accompanied with a high upstream particle velocity, resulting in strong reflection of energy and thus high sound attenuation. Similar phenomenon can be observed at $ka = 2.24$ and other similar frequencies. The situation at $ka \sim 3$ is also very similar, but the strengths of the inward particle velocities on the two sides of the main duct are not equal (not shown here), resulting in less effective reflection.

The corresponding result for the F-type array is very close to that of its L-type counterpart (Fig. 8). However, as shown earlier, the F-type array gives better results at higher frequencies than its L-type counterpart, but the opposite is observed at lower frequencies. The τ variation of the combined array formed by installing a L-type array and a F-type array with $w = 0.1a$, one on each side of the duct, is also presented in Fig. 8. However, the low frequency performance is a bit worse than the combined array formed by two L-type arrays with different w.

It is noted that a discontinuity of τ can be observed in Fig. 8 at $ka \sim 0.4\pi$ for all the abovementioned combined

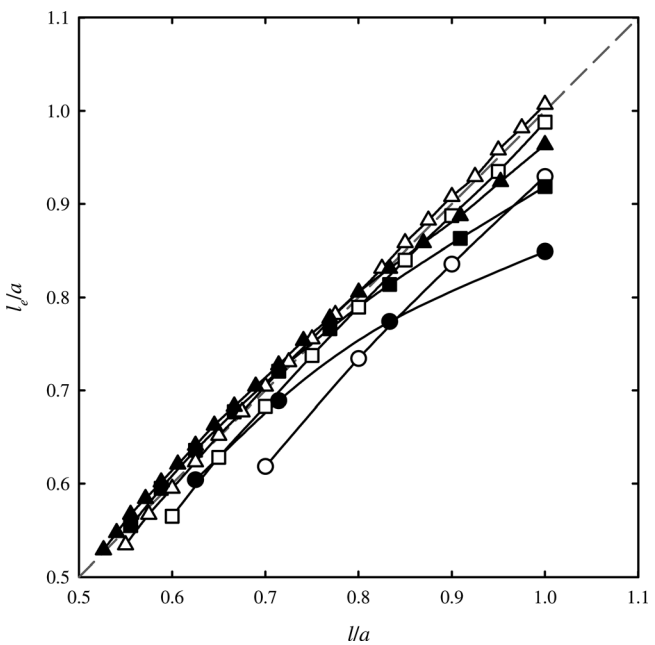

FIG. 7. Effective lengths of sidebranch tubes. Δ, $w = 0.05a$; □, $w = 0.1a$; ○, $w = 0.2a$; - - -, line of $l = l_e$. Open symbols, L-type array; closed symbols, F-type array.

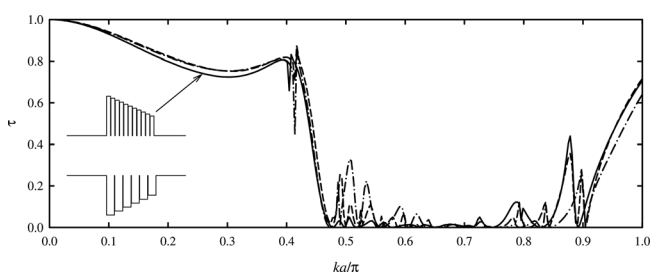

FIG. 8. Sound power transmission coefficients of asymmetric arrays with $w = 0.1a$ and $0.2a$ for the upper and the lower array, respectively, unless otherwise stated. —, L-type arrays; - · -, F-type arrays; - - -, one side L-type and one side F-type with $w = 0.1a$ for both arrays.

array cases. For the L-type array, it takes place at $ka \sim 1.27$. This discontinuity is due to the expansion chamber type transverse mode resonance[27] with the acoustic pressures on the two sides of the main duct in opposite phase (not shown here). The average tube length of the L-type array in Fig. 8 is $0.75a$, and thus the equivalent expansion chamber will has a transverse width L_e of $2.5a$, giving $kL_e = 3.175 \sim \pi$. The corresponding L_e of the F-type array is about $2.4a$, and thus the τ dip appears at a higher frequency with $ka = 1.30$ as shown in Fig. 8.

All the abovementioned arrays are asymmetric about the main duct axis, and thus higher duct modes will be excited for $ka \geq \pi$. The following discussions are focused on the cases of symmetric sidebranch arrays, where the first higher duct mode cut-on is at $ka = 2\pi$. The length of the shortest sidebranch tube of each of these arrays is $0.25a$. The total longitudinal lengths of the arrays, L, can then be as long as $\sim 3.4a$ for $w = 0.2a$.

Figure 10(a) illustrates the frequency variations of τ for three symmetrical L-type arrays with $w = 0.05a$, $0.1a$, and $0.2a$ having longitudinal lengths vary from roughly $1.2a$ to $1.25a$. Therefore the number of sidebranch tubes in each array is different. The sound power transmission coefficients are basically lower than those of their asymmetric counterparts presented in Fig. 5, probably due partially to the expansion chamber effect, which has already been discussed in Figs. 8 and 9. Again a slow varying τ envelope can be observed as a result of the effect of the equivalent expansion chamber.[27] For $ka > \pi$, τ fluctuates over a wide range, and the magnitude of this fluctuation appears to be relatively steady for $ka > 1.8\pi$. One can observe from Fig. 10(a) that τ is relatively low within the narrow range of $1.4 < ka/\pi < 1.8$ for all w studied. As the fundamental resonance wavenumber of first sidebranch tube is $\sim 0.5\pi$ and the frequency of the first harmonic of this resonance is roughly equal to the fundamental resonance frequency of the last sidebranch tube for the adopted symmetric arrays, the abovementioned τ dip at $ka \sim 1.5\pi$ is expected to be due to the concerted resonance effect of these two sidebranch tubes, which tend to create

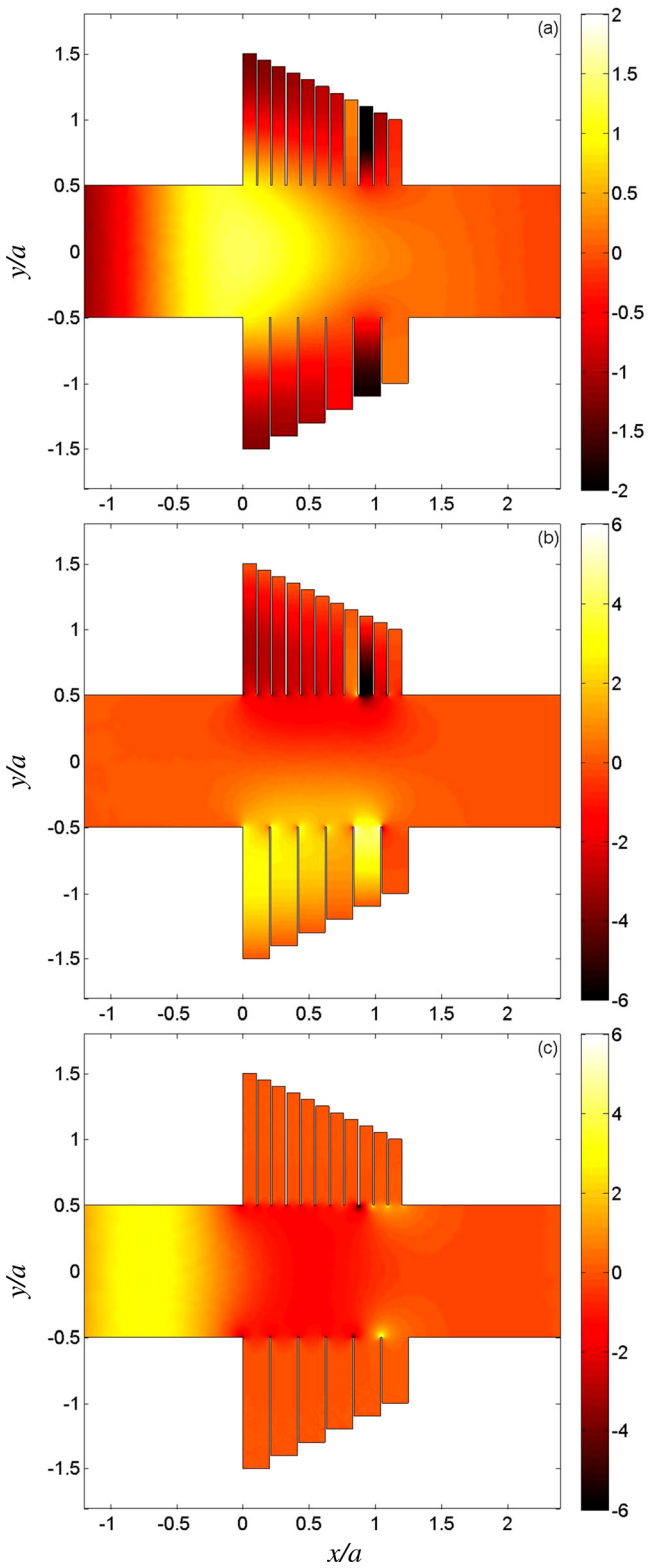

FIG. 9. (Color online) Wave patterns within an asymmetric L-type array formed by a 11- tube L-type array with $w = 0.1a$ and $l_{11} = 0.5$a and a 6-tube L-type array with $w = 0.2a$ and $l_6 = 0.5a$ at $ka = 2.39$. (a) Real part of the acoustic pressure; (b) real part of the transverse acoustical velocity; (c) Real part of the longitudinal acoustical velocity.

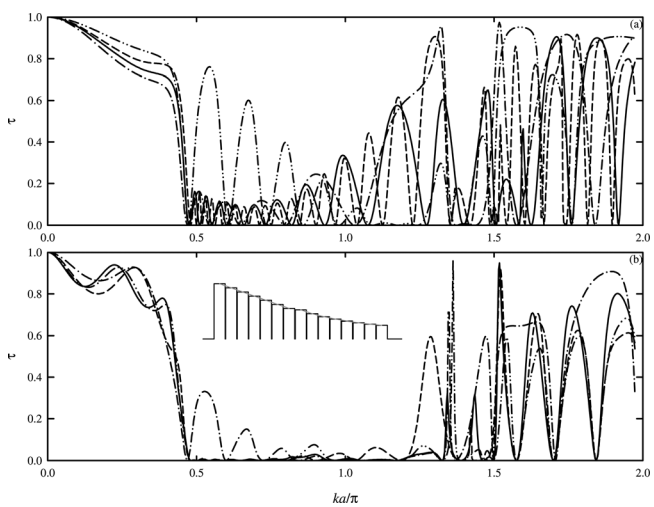

FIG. 10. Sound power transmission coefficients of symmetric arrays. (a) Effects of sidebranch tube width with total array length $\sim 1.2a$ and $l_{min} = 0.5a$ - - -, L-type, $w = 0.05a$, 21 tubes; —, L-type, $w = 0.1a$, 11 tubes; - · -, L-type, $w = 0.2a$, 6 tubes; - · · -, F-type, $w = 0.2a$, 6 tubes. (b) Example of combining L-type and F-type arrays with 11 tubes, $w = 0.2a$ and $l_{11} = 0.25a$. —, "L7+F8" arrangement; - · · -, "L7+F7" arrangement; - - -, L-type; - · -, F-type.

low pressure zones at the exit of the array, resulting in relatively high sound transmission loss.

Figures 11(a) and 11(b) give two examples of the sound fields within the proximity of the L-type array in Fig. 10(a) at $ka = 4.98$ (1.58π) and 5.53 (1.76π), respectively, where high sound transmission loss is observed. At $ka = 4.98$ [Fig. 11(a)], two resonances are observed. One is of the type shown in Fig. 6(b), and the resonance takes place along the third last sidebranch tube of the array. The other one is a first harmonic resonance along the second sidebranch tube. A strong reflection back to the upstream at the entrance of the array section and a strong standing wave within the array section can be observed. For $ka > 5$, only the first harmonic resonance is responsible for the high sound transmission loss. The sound field pattern at $ka = 5.53$, shown in Fig. 11(b), is a typical example. At $ka = 5.53$, the first harmonic resonance appears also along the second sidebranch tube. The effective length of the tube is affected by the fluid loading and the wave activities within the array section.

Also shown in Fig. 10(a) is the τ frequency variation of the F-type array with $w = 0.1a$. Similar to the results of the single sidebranch arrays shown in Fig. 3, the F-type array gives better performance at higher frequencies while the L-type array performs better at lower frequencies. One can then anticipate that a careful combination of these two array types can produce a new symmetrical array that can inherit the advantages of the individual arrays. It is obvious that a sharp change in the tube length variation along the new array will cause an abrupt change in acoustic impedance that is not favorable for broadband sound attenuation as can be inferred from the τ frequency variation of the cubic tube length variation array shown in Fig. 3. To have a smoother transition from a L-type array into a F-type array (that is, wall impedance matching), it is obvious that the lengths of the sidebranch tubes and their axial rates of changes of the two combining arrays at the location of transition should be as close as possible. Figure 10(b) illustrates the frequency variation of τ for a symmetrical array formed by such combination with $w = 0.2a$. The sub-figure in Fig. 10(b) illustrates the array setup. This array consists of seven sidebranch tubes of the L-type and eight sidebranch tubes of the F-type. The τ variations of the corresponding L-type and F-type arrays (11 sidebranch tubes) are also given in Fig. 10(b) for comparison. The transition between the two array forms has inevitably resulted in a very slight deterioration of performance at frequency that is close to the resonance frequencies of the sidebranch tubes at the transition location as the transition/matching is not perfectly smooth unless w is very small. However, the broadband performance is significantly improved. The working wavelength range is about 1.5 times the duct width in this example, and τ within this range is in general less than 0.02 (more than 17 dB *TL*). The performance of the combined array at $ka > 1.5\pi$ resembles more that of the L-type array, indicating that the first seven sidebranch tubes of the L-type are basically controlling the sound transmission at higher frequencies before the cut on of any higher duct modes.

It should be noted that the optimal numbers of L-type sidebranch tubes and F-type tubes in the preceding combination depend on w and the intended working frequency range of the array. The sidebranch tube length variations and the longitudinal rates of change of tube length (dl/dx) of the arrays with 11 tubes, $w = 0.2a$ and $l_{11} = 0.25a$ are presented in Fig. 12(a). One can notice that the dl/dx near to the fourth sidebranch tube of the F-type array is close to that of its L-type counterpart. The length of the fourth tube of the F-type array is close that of the seventh tube of the L-type array, and thus an array formed by the seven sidebranch tubes with linear length variation followed by eight tubes of the linear frequency variation arrangement, denoted as "L7 + F8" will produce the best acoustical performance [Fig. 10(b)]. The performance of "L7 + F7" is still satisfactory but is not as good as that of "L7 + F8"′ within the region of broadband sound attenuation as shown in Fig. 10(b).

Also shown in Fig. 12(a) are the corresponding variations of the arrays with 11 tubes but with $w = 0.1a$ and $l_{11} = 0.5a$. The values of the dl/dx of the F-and L-type arrays are very close at the location of the fifth tube. Because the seventh tube of the linear length variation array is slightly shorter than the fifth tube of the linear frequency variation array, the optimal arrangement in this case will be "L6+F7." This is actually the case (not presented here). Figure 12(b) illustrates the corresponding variations of the combining arrays with 21 tubes, $w = 0.1a$ and $l_{21} = 0.25a$. The optimal arrangement appears to be "L14+F14."

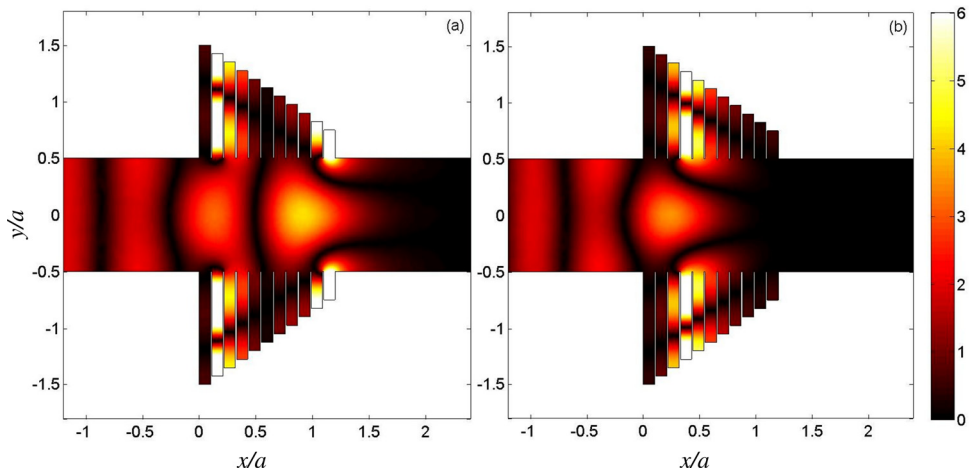

FIG. 11. (Color online) Examples of wave magnitudes inside symmetric L-type array at frequencies of high sound transmission loss within the higher frequency range. $w = 0.1a$, $l_{11} = 0.5a$, 11 tubes a side (a) $ka = 4.98$; (b) $ka = 5.53$.

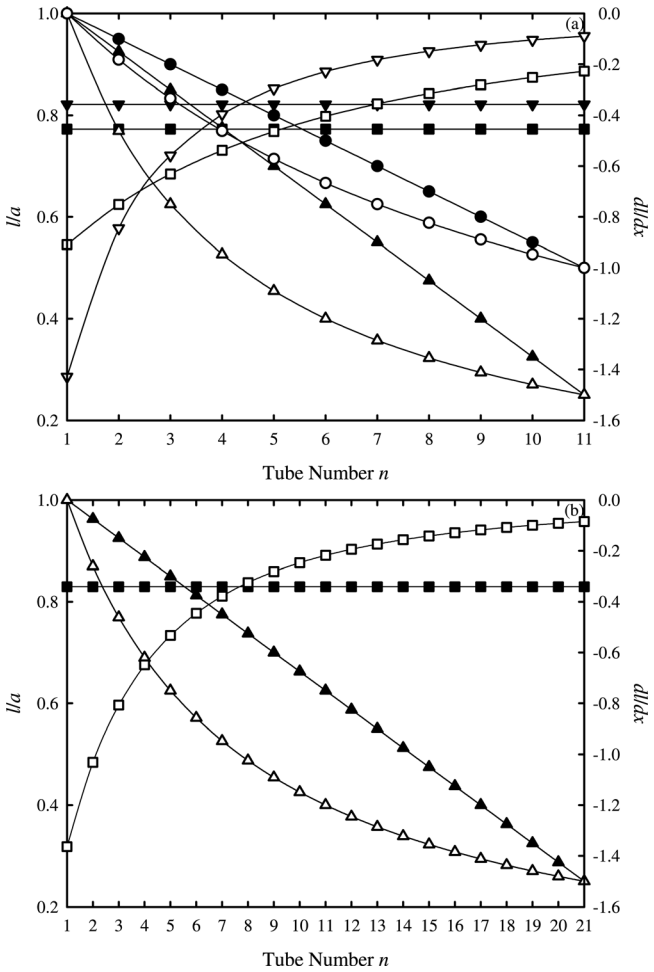

FIG. 12. Matching of L-type and F-type arrays for optimal combinations. (a) 11 tubes a side L-type and F-type combination. ○, l variation, $w=0.1a$, $l_{11}=0.5a$; □, dl/dx variation, $w=0.1a$, $l_{11}=0.5a$; △, l variation, $w=0.2a$, $l_{11}=0.25a$; ▽, dl/dx variation, $w=0.2a$, $l_{11}=0.25a$. (b) 21 tubes a side L-type and F-type combination, $l_{21}=0.25a$, $w=0.1a$. ○, l variation; □, dl/dx variation; open symbols, F-type; closed symbols, L-type.

The present study is focused at frequencies below that of the first higher mode cut-off in the absence of a mean flow in the duct. The mean flow may induce tonal sound as indicated in existing literatures (such as Nelson *et al.*[28] and Ziada *et al.*,[29] but the narrow sidebranch tube width may weaken such lock-on effect.[7] These are left to further study.

V. CONCLUSIONS

The sound transmissions across a duct section with wall-mounted arrays consist of many narrow sidebranch tubes are investigated using mainly the finite-element method in the present study. A simplified theoretical analysis is also given. The effects of various simple tube length arrangements on the sound transmission loss are discussed. The study then focused on the linear tube length variation array and the linear resonance frequency variation array as these two tube length arrangements appear to perform better than some other simple forms considered in this investigation. Apart from the sound transmission properties of a single wall-mounted array, those of double arrays arranged symmetrically and/or asymmetrically about the duct axis are also examined in details.

The results suggest that the sound transmission losses of the arrays, be they are single wall-mounted ones or arranged on opposite duct walls, are high whenever resonance occurs along a particular sidebranch tube, excluding the last two of the arrays. The high sound transmission loss is shown to be due to the combined effect of the monopole radiation of the resonating tube and the dipole-like action of the two consecutive tubes immediately downstream of the resonating one. The expansion chamber effect tends to produce some sound attenuation at the non-resonance frequencies. This effect appears more prominent in the cases of symmetrical arrays, where the out-of-phase transverse acoustical particle velocities on the two sides of the duct axis give additional help on weakening sound transmission. In addition, the present results demonstrate that a wide broadband sound reduction can be achieved by an appropriate sidebranch tube length arrangement. The working frequency band of the device can be greatly enhanced by suitable couplings of arrays on the two sides of the duct. A broadband reduction of more than 17 dB is demonstrated in the present study. Though the present study is a two-dimensional one, the results tend to suggest that further improvement can be done by using all the four walls of a duct.

The present study is focused at frequencies below that of the first higher mode cut-off in the absence of a mean flow in the duct. The effect of higher duct modes on the overall sound transmission characteristics and the effects of turbulent duct flow and viscosity are left to further investigations.

ACKNOWLEDGMENT

This work was supported by a grant from the Research Committee, the Hong Kong Polytechnic University under the Project Number G-U906.

[1]A. Fry, *Noise Control in Building Services* (Pergamon, Oxford, 1988), Chap. 7.
[2]L. L. Beranek, "Criteria for office quieting based on questionnaire rating studies," J. Acoust. Soc. Am. **28**, 833–852 (1956).
[3]W. E. Blazier, "Revised noise criterion for application in the acoustical design and rating of HVAC systems," Noise Control Eng. J. **162**, 64–73 (1981).
[4]C. M. Harris, *Handbook of Noise Control* (McGraw-Hill, New York, 1979), Chap. 29.
[5]G. Canevet, "Active sound absorption in an air conditioning duct," J. Sound Vib. **58**, 333–345 (1978).
[6]L. Huang and Y. S. Choy, "Vibro-acoustics of three dimensional drum silencer," J. Acoust. Soc. Am. **118**, 2313–2320 (2005).
[7]S. K. Tang, "On sound transmission loss across a Helmholtz resonator in a low Mach number flow duct," J. Acoust. Soc. Am. **127**, 3519–3525 (2010).
[8]X. Li and C. H. Hansen, "Comparison of models for predicting the transmission loss of plenum chambers," Appl. Acoust. **66**, 810–828 (2005).
[9]A. Selamet and I. J. Lee, "Helmholtz resonator with extended neck," J. Acoust. Soc. Am. **113**, 1975–1985 (2003).
[10]S. H. Seo and Y. H. Kim, "Silencer design by using array resonators for low frequency band noise reduction," J. Acoust. Soc. Am. **118**, 2332–2338 (2005).
[11]S. Griffin, S. A. Lane, and S. Huybrechts, "Coupled Helmholtz resonators for acoustic attenuation," ASME Trans. J. Vib. Acoust. **123**, 11–17 (2001).
[12]M. B. Xu, A. Selamet, and H. Kim, "Dual Helmholtz resonator," Appl. Acoust. **71**, 822–829 (2010).

[13]T. Kar and M. L. Munjal, "Analysis and design of conical concentric tube resonators," J. Acoust. Soc. Am. **116**, 74–83 (2004).
[14]A. Salemat, N. S. Dickey, and J. M. Novak, "The Herschel-Quincke tube: A theoretical, computational and experimental investigation," J. Acoust. Soc. Am. **96**, 3177–3185 (1994).
[15]C. Q. Howard, B. S. Cazzolato, and C. H. Hansen, "Exhaust stack silencer design using finite element analysis," Noise Control Eng. J. **48**, 113–120 (2000).
[16]S. K. Tang, "Sound transmission characteristics of Tee-junctions and the associated length corrections," J. Acoust. Soc. Am. **115**, 218–227 (2004).
[17]C. K. Lau and S. K. Tang, "Sound transmission across duct constrictions with and without tapered sections," J. Acoust. Soc. Am. **117**, 3679–3685 (2005).
[18]S. K. Lau and K. H. Leung, "Transmission characteristics of a tee-junction in a rectangular duct at higher–order modes," J. Acoust. Soc. Am. **126**, 3028–3039 (2009).
[19]P. E. Doak, "Excitation, transmission and radiation of sound from source distributions in hard- walled ducts of finite length (I): The effects of duct cross-section geometry and source distribution space-time pattern," J. Sound Vib. **31**, 1–72 (1974).
[20]L. Huang, "A theory of reactive control of low-frequency duct noise," J. Sound Vib. **238**, 575–594 (2000).
[21]L. E. Kinsler, A. R. Frey, A. B. Coppens, and J. V. Sanders, *Fundamentals of Acoustics*, 4th ed. (Wiley, New York, 2000), 273 pp.
[22]C. J. Tranter, *Techniques of Mathematical Analysis* (Hodder and Stoughton, London, 1980), 198 pp.
[23]D. Tonon, J. F. H. Willems, and A. Hirschberg, "Self-sustained oscillations in pipe systems with multiple deep side branches: Prediction and reduction by detuning," J. Sound Vib. **330**, 5894–5912 (2011).
[24]S. K. Tang, C. H. Ng, and E. Y. L. Lam, "Experimental investigation on the sound absorption performance of compartmented Helmholtz resonators," Appl. Acoust. **73**, 969–976 (2012).
[25]L. Langemyr, A. Nordmark, M. Ringh, A. Ruhe, J. Oppelstrup, and M. Dorobantu, *Partial Differential Equation Toolbox User Guide* (The MathWorks, Natick, MA, 2009). Also available at http://www.kxcad.net/cae_MATLAB/toolbox/pde/ug/assempde.html (Last viewed 1/24/2012).
[26]L. P. George, *Automatic Mesh Generation—Application to Finite Element Methods* (Wiley, New York, 1991), Chaps. 3 and 13.
[27]C. K. Lau and S. K. Tang, "Mode interactions and sound power transmission loss of expansion chambers," ASME Trans. J. Acoust. Vib. **129**, 141–147 (2007).
[28]P. A. Nelson, N. A. Halliwell, and P. E. Doak, "Fluid dynamics of a flow excited resonance, Part II: Flow acoustic interaction," J. Sound Vib. **91**, 375–402 (1983).
[29]S. Ziada, H. Ng, and C. E. Blake, "Flow excited resonance of a confined shallow cavity in low Mach number flow and its control," J. Fluids Struct. **18**, 79–92 (2003).